Tuning the Refractive Index of Homopolymer Blends by Controlling Nanoscale Domain Size via RIR-MAPLE Deposition

Ryan D. McCormick, Eric D. Cline, Arvinder S. Chadha, Weidong Zhou, Adrienne D. Stiff-Roberts*

Anti-reflection (AR) coatings designed for glass and other rigid, inorganic substrates are commercially available; however, these inorganic AR coatings tend to crack or delaminate on flexible substrates. A polymeric film with a gradient refractive index (GRIN) profile would make an ideal AR coating for flexible substrates, but such coatings are challenging to fabricate using traditional, solution-based techniques. Emulsion-based resonant infrared, matrix-assisted pulsed laser evaporation (RIR-MAPLE) offers a straightforward approach to enabling the desired GRIN profile in polymeric materials. Two homopolymers (polystyrene (PS) and poly(methyl methacrylate) (PMMA)) are deposited as a blend and one component (PMMA) is dissolved, leaving behind a porous PS film. The porosity and refractive index (RI) are controlled by the volume ratio of the two homopolymers in the film. Structural and optical characterizations, as well as comparison to modeled optical properties, confirm that porous films fabricated from polymer blends deposited by RIR-MAPLE behave as effective media over most of the visible spectrum. While evidence for the partial collapse of the porous polymer networks is observed, the RI of the porous films is reduced from that of the bulk material. Importantly, these studies demonstrate that RIR-MAPLE should enable broadband, omnidirectional, polymeric AR coatings appropriate for flexible substrates.

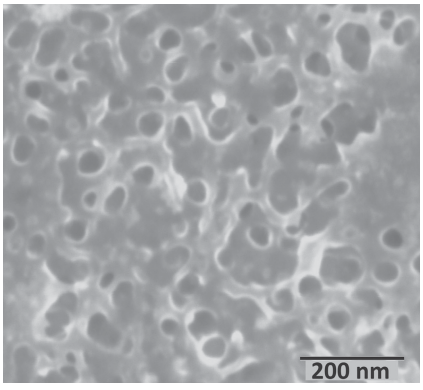

1. Introduction

Most anti-reflection (AR) coatings, used in applications such as flat screen displays, solar cells, or eyeglasses,[1] are produced for glass substrates by physical or chemical vapor deposition of metal oxides or metal fluorides. However, when deposited on flexible organic substrates, such as plastics, these inorganic AR coatings experience cracking and delamination because of the mismatch between the coefficients of thermal expansion (CTE) for the AR coating and the plastic substrate. Therefore, polymeric AR coatings with materials properties that are compatible with organic, flexible substrates are required for current and emerging technologies, such as flexible flat panel displays[2] and plastic lens eyeglasses.[3]

A truly broadband, omnidirectional, and polymeric AR coating would be ideal, but such a film is challenging because it requires grading the refractive index (RI) from that of the organic substrate (e.g., polycarbonate with n = 1.5–1.6) to that of the surrounding medium (usually air with n = 1.0). Solution-cast polymeric porous films have been reported as organic, gradient refractive index (GRIN),

R. D. McCormick
Department of Electrical and Computer Engineering
Duke University, Durham, NC 27708, USA
Dr. E. D. Cline
ZT Solar, Inc., Dallas, TX 75235, USA
A. S. Chadha, Prof. W. Zhou
Department of Electrical Engineering, University of Texas at Arlington, Arlington, TX 76019, USA;
Prof. A. D. Stiff-Roberts
Department of Electrical and Computer Engineering,
Duke University, Durham, NC 27708, USA
E-mail: adrienne.stiffroberts@duke.edu

DOI: 10.1002/macp.201300465

AR coatings; yet, the graded structure actually consists of several, discrete stacked layers of single refractive index as opposed to a GRIN profile.[4] Similarly, layered nanocomposites of a polymer and oxide nanoparticles have been demonstrated by RIR-MAPLE to reduce the reflectance of a flexible substrate through the visible region.[5] Both demonstrations highlight a significant challenge to realizing a GRIN profile in polymeric films, that is, the required capability to continuously vary the RI over a given film thickness. For example, moth eye nanostructures that feature tapered polymer nanopillars have demonstrated GRIN profiles because the air content increases with decreasing nanopillar diameter from base to tip.[6]

The first roadblock to overcoming this challenge to a polymeric GRIN film is that bulk polymers cannot achieve RI values significantly below the theoretically determined limit of $n = 1.29$.[7] However, low RI polymeric materials can be achieved as an optical effective medium, that is, by incorporating a low index component into a higher index polymer matrix. For example, nanocomposites of metal nanoparticles within a polymer matrix can lower the RI to less than 1.0 through the visible range.[8] Air can also be incorporated as a low index component via porous films.[4] In fact, networks of porous polymers constitute an attractive option for low RI films due to their simplicity: a blend of two polymers is deposited onto a substrate, after which one component (porogen) is chemically dissolved, leaving a 3D network of polymer and air pores. The constituent domain sizes of the polymer blend are critical, in this case, because they determine the light scattering characteristics of the overall film.

The deposition of a polymeric, optical effective medium is not straightforward using traditional, solution-based techniques, however, because the polymer blend tends to segregate into large, micron-sized domains. Solution-cast films of polymer blends often require the employment of diblock copolymers with tailored block sizes or substrate surface treatments that drive homopolymer blending in order to approach an effective medium.[4] In contrast, emulsion-based resonant infrared matrix-assisted pulsed laser evaporation (RIR-MAPLE) is an organic thin-film deposition technique (variation of pulsed laser deposition) that is capable of creating a polymeric, optical effective medium with a specific RI due to nanoscale domains[9] within the polymer blend. Therefore, this paper demonstrates emulsion-based RIR-MAPLE as a technique to enable porous polymer networks with a specified RI that is designed using effective medium theory and is lower than those of the constituent materials in the polymer blend. Importantly, using emulsion-based RIR-MAPLE to achieve a polymeric, optical effective medium is the first step towards realizing a truly broadband, omnidirectional, AR coating appropriate for plastic substrates by enabling a polymeric GRIN profile.

2. Emulsion-Based RIR-MAPLE of Homopolymer Blends

It is important to note that MAPLE deposition of polymer blends has been reported previously. UV-MAPLE, featuring an ultraviolet Nd:YAG laser ($\lambda = 266$ nm), has been used to deposit blends of poly(ethylene glycol) (PEG) and poly(lactide-*co*-glycolide) (PLGA) for medical applications, such as drug delivery or intraocular lenses.[10,11] The refractive index of these UV-MAPLE-deposited polymer-blend films shows some dependence on the polymer-blend ratios, yet, the novelty and significance of the work reported herein is that desired RI values lower than those achievable with bulk polymers are defined in advance, and the emulsion-based RIR-MAPLE growth is designed to achieve these target values.

Organic thin-film deposition by emulsion-based RIR-MAPLE has been discussed in detail elsewhere,[12,13] but it is important to note that the unique approach of this deposition technique is the use of water ice as the majority host matrix. This matrix choice results from the laser system, a table-top Er:YAG laser with a fixed emission wavelength at 2.94 μm that is resonant with hydroxyl (O–H) bonds. By creating target emulsions of the desired guest material and corresponding solvent with water, emulsion-based RIR-MAPLE deposition of a variety of polymers, nanoparticles, and hybrid organic/inorganic nanocomposites has been demonstrated.[14,15] It has also been shown that emulsion-based RIR-MAPLE deposits polymers with negligible change in molecular weight, as compared with other laser deposition techniques,[16] because it resonantly excites a specific molecular vibrational mode of the host matrix (water ice) that is absent from the guest material. Crucially, the majority of organic materials germane to photonic and optoelectronic applications do not contain O–H bonds in positions within their chemical structure that are vital for proper functionality, thereby allowing RIR-MAPLE a wide range of potential materials for deposition. As a result, emulsion-based RIR-MAPLE can deposit polymer blends simultaneously, regardless of the solubility match of the materials. This technique can also achieve a wide range of material ratios in the blended film simply by varying the ratio of the materials during deposition. The multi-layer capability of RIR-MAPLE has been demonstrated by the successful fabrication and characterization of a 16-layer, all-polymer distributed Bragg reflector in the near IR region.[17] Therefore, in contrast to solution-based deposition, emulsion-based RIR-MAPLE demonstrates the versatility required for the fabrication of complex structures, such as porous films with a GRIN profile resulting from 3D control over the film morphology (namely control over polymer-blend domain sizes and ability to continuously vary polymer-blend ratios over a given film thickness).

Thus, as a first step, emulsion-based RIR-MAPLE is used to achieve a polymeric, optical effective medium by depositing films of a polymer blend (e.g., two homopolymers, polystyrene (PS) and poly(methyl methacrylate) (PMMA)) with different constituent ratios. Details of RIR-MAPLE deposition, in general, have been published elsewhere.[12,13,15] For this work, three ratios by volume of PS:PMMA are chosen: 3:1, 1:1, and 1:3. The PS layer is cross-linked using ultraviolet (UV) light, and the PMMA component (porogen) is removed, leaving a nanoporous, 3D, PS polymer network as the remaining film. The use of porous structures to achieve a specific RI value less than that of a bulk film requires that the domain sizes be significantly less than the wavelength of incident light. A rule of thumb for an optical effective medium is that the domains must be 10 times smaller than the wavelength of interest.[18] When this domain size condition is satisfied, light scattering is avoided and the light wave experiences the heterogeneous medium, effectively, as a homogeneous medium with material properties that are a mixture of the constituent materials. As long as the pores sizes remain below this threshold, small variations in the distribution of pore sizes should have little effect on the refractive index. Therefore, Bruggeman's effective medium theory,[19] shown in Equation 1, is used to determine the correct volume ratio between PS and PMMA that yields a desired effective RI after the PMMA component is dissolved:

$$f\frac{n_a^2 - n^2}{n_a^2 - 2n^2} + (1-f)\frac{n_{ps}^2 - n^2}{n_{ps}^2 - 2n^2} = 0 \quad (1)$$

where f is the volume fraction of air pores; $(1 - f)$ is the volume fraction of the PS network; n_a is the RI of air (1.0), n_{ps} is the RI of PS ($n_{ps} = 1.590$ at $\lambda = 600$ nm), and n is the effective RI of the porous film. Using the Bruggeman formula (Equation 1), the three PS:PMMA volume ratios under investigation (3:1, 1:1, and 1:3) correspond to nominal porosities (i.e., volume fractions of air) of 25%, 50%, and 75%, respectively. As an example, the corresponding calculated effective RI values at 600 nm are 1.402, 1.306, and 1.166, respectively.

Surface characterization and film thickness measurements of the as-deposited and porous films are conducted using scanning electron microscopy (SEM), atomic force microscopy (AFM), and surface profilometry. Optical characterization of bare Si substrates and porous PS films deposited on Si are conducted using spectroscopic ellipsometry (SE) and reflectivity measurements with an integrating sphere. These measured optical properties are compared with calculated optical properties in order to confirm that emulsion-based RIR-MAPLE achieves the desired RI values and affects a reduction in the substrate reflectivity. In addition, the calculated reflectivity can verify that the porous PS film deposited by RIR-MAPLE behaves as an optical effective medium. The calculated reflectivity assumes homogeneous media; therefore, experimental deviation from the theoretical reflectivity spectrum should be indicative of the extent to which the porous films deviate from an effective medium. Importantly, these studies demonstrate that RIR-MAPLE enables porous films with tailored RI using only homopolymers.

3. Results and Discussion

Table 1 outlines the film thicknesses of the blended homopolymer films before and after PMMA removal, as measured independently by both AFM and profilometer. The thickness values from the two separate measurements of porous films are consistent. The as-deposited films had thicknesses of approximately 150–200 nm; after PMMA removal, the porous PS films are all less than 100 nm. Furthermore, the ratio of the porous-to-as-deposited film thickness (determined using the average of the profilometer and AFM thickness measurements), roughly corresponds to the amount of PS in the porous film. For example, in the 75% porous film, the PS:Air thickness was 26% of the as-deposited, PS:PMMA thickness, corresponding to the 25% PS content of the porous film. This is not surprising because it indicates that the reduction in thickness results from partial pore collapse of the films after PMMA removal. This conclusion is also supported by the optical characterization.

SEM images of the film surfaces for the porous PS films on Si are shown in Figure 1. SEM images of the as-deposited films prior to PMMA removal were also collected (see Supporting Information). The film surfaces were

Table 1. Polymer film thicknesses before and after dissolution and removal of the PMMA component. AFM error is deviation from mean of multiple measurements. Profilometer error is the RMS surface roughness along a 100 μm line on the film.

Porosity [%]	PS:PMMA Film Thickness, AFM [nm]	PS:Air Film Thickness, Profilometer [nm]	PS:Air Film Thickness, AFM [nm]	Porous/As-deposited Thickness [%]
25	162 ± 18	89 ± 17	88 ± 9	55
50	149 ± 8	65 ± 10	70 ± 3	45
75	184 ± 11	49 ± 12	46 ± 3	26

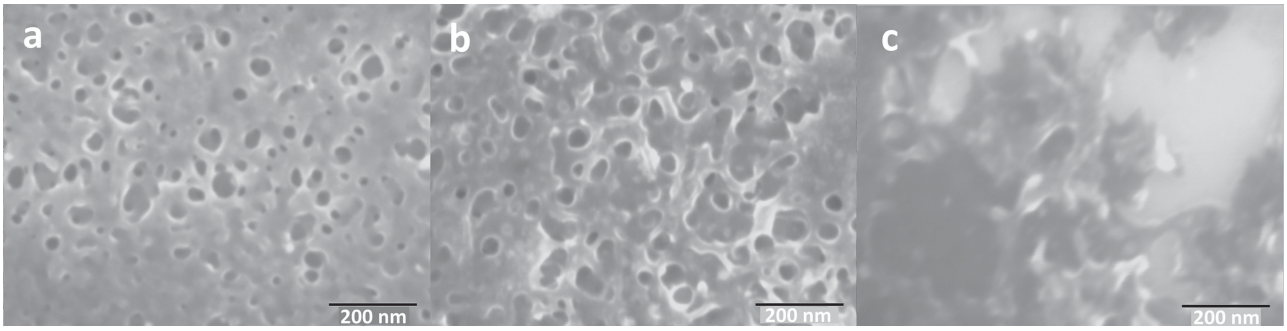

Figure 1. SEM images of porous polystyrene films: a) 25% porosity, b) 50% porosity, c) 75% porosity.

featureless and began to charge at magnifications less than that of the images of Figure 1. A TEM image of the RuO_4-stained film, which clearly shows the separate PS and PMMA components of the blend, has been published elsewhere.[9] The SEM images for the 25%, 50%, and 75% porosity films, shown in Figure 1a–c, respectively, clearly demonstrate that the porosity increases as the PMMA content increases in the blended homopolymer films deposited by RIR-MAPLE. The 75% porous film of Figure 1c has so little PS remaining after PMMA removal that pore collapse at the surface is evident. Nevertheless, the pores closer to the substrate are most likely intact, as demonstrated by the optical characterization of the porous films. It is evident in the SEM images that the average pore size is of the order of 50 nm, satisfying the effective medium criterion that the pore size must be of the order of 10% or less of the incident wavelength. Therefore, these porous films meet the effective medium requirements for the majority of the visible spectrum.

The RI values of the porous PS films, measured by SE (from 400–800 nm), are shown using data points in Figure 2 (25% porosity – circles, 50% porosity – triangles, and 75% porosity – squares). The measured bulk polystyrene RI spectrum[20] is also shown as a reference. For each porosity, the RI value as a function of incident light wavelength, λ, is calculated using the Sellmeier equation for comparison[21] (see Supporting Information for the Sellmeier coefficients that result from fitting the measured RI). The theoretical RI dispersion curves are represented by the solid lines in Figure 2. The expected trend is observed in the RI data: as the porosity increases, the RI decreases as more air is introduced into the film composition. The RI values calculated using Bruggeman effective medium theory at 600 nm are 1.402, 1.306, and 1.166, for 25%, 50%, and 75% porosities, respectively; and, the experimental values are 1.413, 1.336, and 1.218, respectively. The increasing disparity between the predicted and experimental values with increasing porosity implies an increasing amount of pore collapse as the amount of solid material is decreased in the 3D network and the structural stability is decreased.

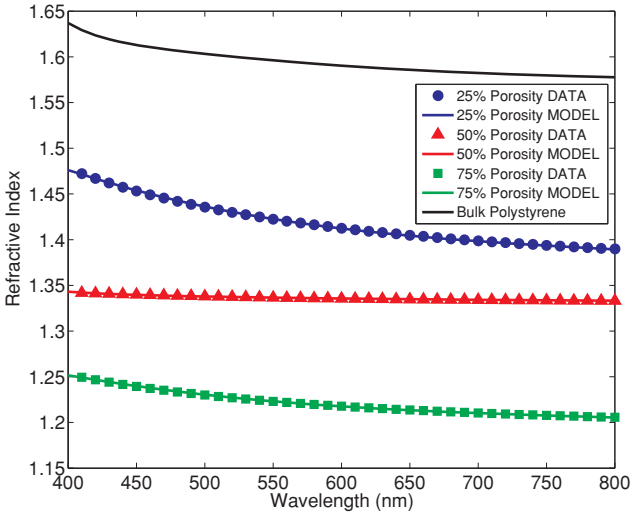

Figure 2. Refractive index spectra of porous polystyrene films as measured by spectroscopic ellipsometry. Experimental data points are shown relative to bulk polystyrene (black line); Sellmeier fits to the experimental RI data are represented as solid lines. Fitting coefficients are given in the supplemental materials.

The issue of pore collapse is also explored by comparing the measured and calculated reflectivity spectrum for each sample with different porosity (using the bare silicon substrate as a reference). At normal incidence to the film, the condition under which reflectivity measurements were made, the reflectivity is given by a simple Fresnel transfer matrix approach for a single homogeneous film on a homogeneous substrate, surrounded by air:

$$R(\lambda, n, d, \theta = 0^\circ) = \frac{n^2(n_a - n_{ps})^2\left[\cos\left(\frac{2\pi}{\lambda} nd\right)\right]^2 + (n_a n_{ps} - n^2)^2\left[\sin\left(\frac{2\pi}{\lambda} nd\right)\right]^2}{n^2(n_a - n_{ps})^2\left[\cos\left(\frac{2\pi}{\lambda} nd\right)\right]^2 + (n_a n_{ps} - n^2)^2\left[\sin\left(\frac{2\pi}{\lambda} nd\right)\right]^2} \quad (2)$$

where λ represents the wavelength of the incident light, d is the film thickness, θ is the light incidence angle relative to the substrate normal, and n_a, n_{ps}, and n, are the dispersive RI values of air, polystyrene, and the porous film, respectively. The reflectivity is very sensitive to film thickness and incident light wavelength, as demonstrated in Figure 3a,b, in which the reflectivity for a 50% porous PS

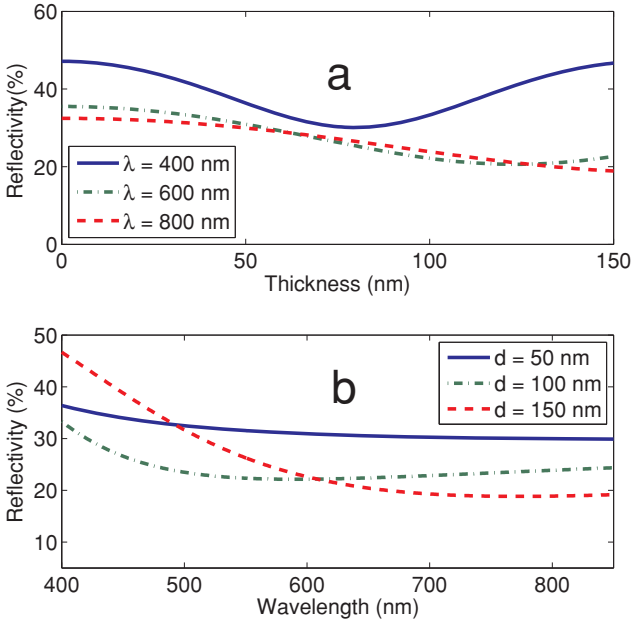

Figure 3. Calculated reflectivity spectra of porous polystyrene thin films (50% porosity by volume). a) Film thickness effects for three different incident wavelengths (400 nm, 600 nm, 800 nm). (b) Spectral effects for three film thicknesses (50 nm, 100 nm, and 150 nm).

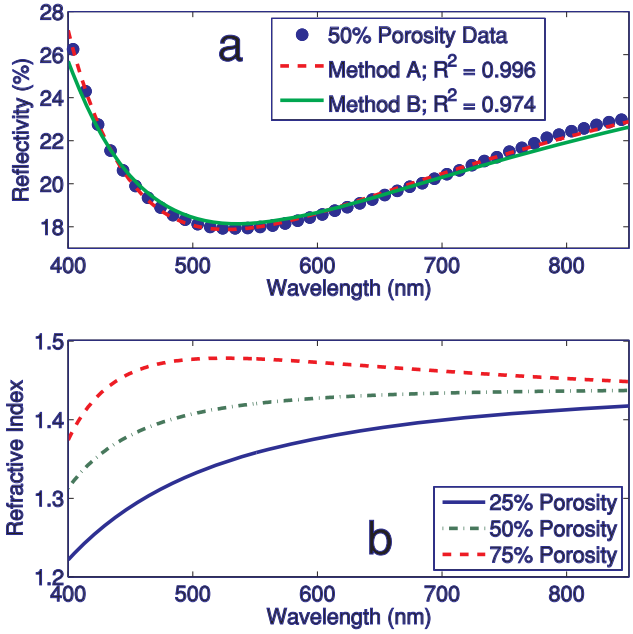

Figure 4. a) Comparison of measured and fit (Methods A and B) reflectivity spectra for 50% porous polystyrene film. The red curve represents Method A, which results in an RI spectrum with anomalous dispersion that is non-physical (see Figure 4b). The green curve represents Method B, which is the true physical representation of the film. b) Non-physical refractive index spectra that resulting from fitting the measured reflectivity using Method A. The corresponding porosities trend in the wrong direction with respect to the RI value. Also, the RI shape demonstrates anomalous dispersion, yet normal dispersion is observed in the measured ellipsometry data.

film is calculated as a function of d and λ, respectively. The RI value for n used to calculate the reflectivity is that measured by SE for the PS film with 50% porosity. In Figure 3a, the calculated reflectivity is plotted as a function of film thickness for three different incident wavelengths (400 nm, 600 nm, 800 nm); while in Figure 3b, the calculated reflectivity is plotted as a function of incident wavelength for three different film thicknesses (50 nm, 100 nm, 150 nm). These plots demonstrate that an intuitive trend of reflectivity versus porosity cannot be determined directly because of the variations that occur due to incident wavelength or film thickness. Rather, the reflectivity data is analyzed by determining the quality of the fit between the measured and calculated reflectivity for each specific sample.

As seen in Equation 2, the RI dispersion of the porous films, $n(\lambda)$, and the film thickness, d, are the two primary experimental parameters that determine the calculated reflectivity. Therefore, two possible approaches are pursued in order to compare the measured and calculated reflectivity spectra for the porous films: 1) Method A: let d equal the measured film thickness (by AFM or profilometer) and determine $n(\lambda)$ by fitting the measured and calculated reflectivity; or 2) Method B: let $n(\lambda)$ equal the measured RI dispersion (by SE) and determine d by fitting the measured and calculated reflectivity. A nonlinear least squares fitting routine is used in each case. Figure 4a shows examples of the two approaches to fitting the measured and calculated reflectivity spectra for the 50% porosity film. The blue circles represent the measured reflectivity data, the red curve represents the calculated reflectivity spectrum for Method A, and the green curve represents the calculated reflectivity spectrum for Method B. For the red curve, the R^2 value that indicates the goodness of the fit is approximately unity, but the RI that results from fitting the measured and calculated reflectivity spectra, shown as the blue curve in Figure 4b, is not physical. In fact, Figure 4b demonstrates that the RI dispersion, $n(\lambda)$, determined by Method A is non-physical for each film porosity due to the anomalous dispersion that is not observed in the measured ellipsometry data. Additionally, the RI values trend in the wrong direction for the given porosities; for example, the 75% film porosity should yield the lowest RI and the 25% film porosity should yield the highest RI. However, by using Method B, some insight into the film integrity can be achieved.

Figure 5 shows the measured reflectivity (data points) compared to the calculated reflectivity determined using Method B (solid lines) for each sample porosity. It is

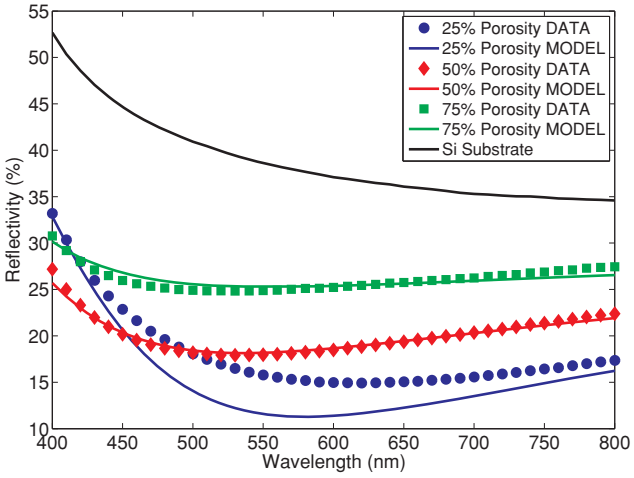

Figure 5. Measured reflectivity spectra (using integrating sphere) of the RIR-MAPLE-deposited porous polystyrene films (i.e., after PMMA removal). Markers depict experimental data relative to the Si substrate (black line); solid lines represent the Fresnel transfer matrix model fit to the measured data using Method B.

apparent that all of the samples reduce the reflected light relative to the substrate alone, and that the calculated reflectivity shows a reasonable fit to the measured reflectivity data. To be specific, the reflectivity of the bare silicon substrate at 600 nm is 37.2%, and this measured value reduces to 15.0%, 18.5%, and 25.2%, for the PS films with 25%, 50%, and 75% porosity, respectively. However, as cautioned in the discussion of Figure 3, this reflectivity trend with porosity at a single wavelength cannot be generalized because the film thicknesses vary for each sample.

This issue is explored further by comparing the measured and fit film thicknesses determined using Method B for each film porosity. For the 25%, 50%, and 75% porosity films, the average film thickness was measured to be 89 nm, 69 nm, and 46 nm, respectively, while the thickness determined by fitting the reflectivity is 97.4 nm, 82.5 nm, and 79.8 nm, respectively. The R^2 values are 0.504, 0.974, and 0.752 for the fits to the 25%, 50%, and 75% porosity films, respectively. As the nominal porosity increases, the measured and the fit values of the film thickness diverge, with a 25% porous film having only 8 nm difference, while the 75% porous film has a 34 nm span that indicates more severe pore collapse. As another check of the measured data, Bruggeman's effective medium theory (Equation 1) is used to determine the effective porosity that accounts for the observed pore collapse. Analytical expressions for the dispersive RI values of air and polystyrene were calculated from the Sellmeier equation based on independent RI data of air and polystyrene.[22] These analytical expressions were used in conjunction with Equation (1) to fit the measured RI of the porous films, and the effective porosity (i.e., volume fraction of air) is extracted as a fitting parameter. The results demonstrate that the effective porosities follow the same general trend as the targeted porosity: namely, 28.8%, 41.8%, and 60.9% calculated porosities for the 25%, 50%, and 75% nominal porosities, respectively. In addition, these effective porosity values provide a measure of the integrity of the pore structure. As the porosity increases, or as the corresponding RI decreases, the reduction of the effective porosity compared to the corresponding targeted value indicates an increase in the occurrence of pore collapse, a trend mirrored by the difference between the measured and fit film thicknesses.

4. Conclusion

A polymeric, optical effective medium featuring a blend of two different homopolymer components, PS, and PMMA, has been deposited using emulsion-based RIR-MAPLE. Removal of the PMMA component after UV cross-linking of the PS component leaves a porous PS film that yields a decrease in reflectivity relative to a bare silicon substrate. Importantly, these porous films have been shown to behave as effective media for the majority of the visible spectrum. In addition, the corresponding RI value can be tuned from that of the bulk PS material near 1.59 to values below those achievable with bulk materials only. In this study, an RI of 1.20 in the visible region was achieved with the highest porosity film (75%). It should be possible to achieve an RI value closer to that for air in the polymer films by preventing collapse of the porous structures. Future work will focus on making the porous PS structures more stable and durable.

The demonstrated nanoscale polymer-blend domain sizes provided by emulsion-based RIR-MAPLE opens the technique and polymeric materials to a wide variety of applications. For example, optical effective media are useful beyond the AR coatings based on a GRIN profile[4] that provide the motivation for this work. The ability to tailor the constitutive parameters of blended polymer films could enable optical coatings and components[23] using novel materials, such as those that use the photorefractive effect where the domain sizes and constituent mixing are critical.[24] Porous scaffolds, which are applicable as fuel cells, aerogels,[25,26] or catalysts,[27] are another area where nanoscale domain size plays an important role. For example, in catalytic processes, the pore size determines the flow rate and surface area of the reactants that contact the porous catalyst.[27] RIR-MAPLE can also facilitate multifunctional materials by blending two or more materials, each of which contains at least one desired quality of a multifunctional, composite material. For example, in the case of materials for drug release, one material may help with drug release (PEG), while the second material hinders drug release (PLGA). By

controlling the domain size of each material in a blended film, the diffusion of the drug within the blend[28] can be controlled. Thus, the capability of emulsion-based RIR-MAPLE to deposit blended polymer films with nanoscale domains helps resolve fundamental challenges faced by solution-based deposition and broadens the application of polymeric materials for functional thin films and coatings.

5. Experimental Section

5.1. Materials

The PS (molecular weight, $\overline{M}_w$ = 35 000 g mol^{-1}) and PMMA ($\overline{M}_w$ = 10 000 g mol^{-1}) polymers were purchased from Sigma–Aldrich and were directly used without further purification.

5.2. RIR-MAPLE Film Deposition

The polymers were each dissolved in toluene, and then mixed with benzyl alcohol and water to create an emulsion. Each emulsion was flash frozen at −196 °C in the pre-cooled target cup of the RIR-MAPLE system. A pulsed Er:YAG laser (λ = 2.94 μm) provided a 2-Hz, 1.46 J cm^{-2} pulse train (90 μs) that deposited the polymer onto the substrate. All of the films were deposited on silicon substrates to facilitate characterization via SE, atomic force microscopy (AFM), scanning electron microscopy (SEM), and reflectivity measurements. Each deposition was 5 h long, the silicon substrate was positioned 5 cm from the target, and the substrate temperature was held constant at 20 °C.

5.3. PS Cross-linking and PMMA Removal

After deposition, the PS component was cross-linked by exposing the film under vacuum to UV light. The PMMA component of the blended homopolymer films was dissolved by dipping each film into glacial acetic acid for 5 min, after which they were rinsed with deionized water and allowed to dry prior to characterization.

5.4. Structural Characterization

The SEM measurements were conducted using an FEI XL30 FEG at an accelerating voltage of 3 kV at a working distance of 5–6 mm and 300 000× magnification. An attempt to coat the films in gold resulted in the gold filling the pores of the films. Therefore, the images were taken with the native films, but the substrates were grounded with copper tape to reduce charge accumulation. The AFM measurements were conducted using a Digital Instruments Dimension 3100 with Bruker TESP silicon tips with 42 N m^{-1} spring constant and 8–12 nm tip radius. An AlphaStep IQ was used for the profilometer measurements.

5.5. Optical Characterization

An HS-190, variable angle spectroscopic ellipsometer (VASE) by J. A. Woollam Co. was used to extract the ellipsometric data in the wavelength range 400–800 nm in steps of 10 nm. The spectroscopic ellipsometric data were averaged over multiple angles of incidence from 65°–75° in steps of 5°. WVASE32 software was used to model the optical constants of film thickness and refractive index of the porous homopolymer films. The reflectivity was measured at normal incidence by a JASCO V-570 spectrophoto meter with an attached integrating sphere that measures the light reflected by the sample from all directions.

Supporting Information

Supporting Information is available from the Wiley Online Library or from the author.

Acknowledgements: This work was supported by the U.S. Air Force STTR Program (Grant No. FA8650–13-C-5001).

Received: July 10, 2013; Revised: August 13, 2013; Published online: September 20, 2013; DOI: 10.1002/macp.201300465

Keywords: effective media; homopolymers; matrix-assisted pulsed laser evaporation (MAPLE); porous films; refractive index

[1] L. Martinu, D. Poitras, *J. Vac. Sci. Technol. A* **2000**, *18*, 2619.
[2] G. P. Crawford, *Flexible Flat Panel Displays*, John Wiley & Sons, Ltd, Chichester, UK **2005**.
[3] U. Schulz, U. B. Schallenberg, N. Kaiser, *Appl. Opt.* **2002**, *41*, 3107.
[4] X. Li, J. Gao, L. Xue, Y. Han, *Adv. Funct. Mater.* **2010**, *20*, 259.
[5] S. Singaravalu, D. C. Mayo, H. K. Park, K. E. Schriver, R. F. Haglund, *Proc. SPIE 8607, Laser Applications in Microelectronic and Optoelectronic Manufacturing (LAMOM) XVIII* **2013**, 860718.
[6] B.-J. Bae, S.-H. Hong, E.-J. Hong, H. Lee, G.-y. Jung, *Jpn. J. Appl. Phys.* **2009**, *48*, 010207.
[7] W. Groh, A. Zimmermann, *Macromolecules* **1991**, *24*, 6660.
[8] L. Zimmermann, M. Weibel, W. Caseri, U. W. Suter, P. Walther, *Polym. Adv. Technol.* **1993**, *4*, 1.
[9] R. D. McCormick, E. D. Cline, A. S. Chadha, W. Zhou, A. D. Stiff-Roberts, *Proc. SPIE 8258 Org. Photonic Mater. Devices XIV*, **2012**, p. 825806.
[10] I. A. Paun, V. Ion, A. Moldovan, M. Dinescu, *Appl. Phys. Lett.* **2010**, *96*, 243702.
[11] I. A. Paun, V. Ion, A. Moldovan, M. Dinescu, *Appl. Surf. Sci.* **2011**, *257*, 5259.
[12] R. Pate, K. R. Lantz, A. D. Stiff-Roberts, *IEEE J. Sel. Top. Quantum Electron.* **2008**, *14*, 1022.
[13] R. Pate, A. D. Stiff-Roberts, *Chem. Phys. Lett.* **2009**, *477*, 406.
[14] R. Pate, K. R. Lantz, A. Dhawan, T. Vo-Dinh, A. D. Stiff-Roberts, *AIP Conf. Proc.* **2010**, *1278*, 812.
[15] R. Pate, R. McCormick, L. Chen, W. Zhou, A. Stiff-Roberts, *Appl. Phys. A: Mater. Sci. Process.* **2011**, *105*, 555.
[16] R. D. McCormick, J. Lenhardt, A. D. Stiff-Roberts, *Polymers* **2012**, *4*, 341.
[17] R. Pate, *Ph.D. Dissertation*, Electrical and Computer Engineering, Duke University, Durham, USA, **2011**.
[18] G. B. Smith, *Appl. Phys. Lett.* **1979**, *35*, 668.
[19] M. Khardani, M. Bouaïcha, B. Bessaïs, *Phys. Status Solidi C* **2007**, *4*, 1986.

[20] S. N. Kasarova, N. G. Sultanova, C. D. Ivanov, I. D. Nikolov, *Opt. Mater.* **2007**, *29*, 1481.
[21] A. Miller, in *Handbook of Optics: Optical Properties of Materials, Nonlinear Optics, Quantum Optics, Volume 4, 3rd Ed.*, McGraw-Hill Professional Publishing, New York **2009**, p. 8.14.
[22] M. Xiaoyan, Q. L. Jun, R. S. Brock, M. J. Kenneth, Y. Ping, H. Xin-Hua, *Phys. Med. Biol.* **2003**, *48*, 4165.
[23] R. F. Souza, M. A. R. C. Alencar, E. C. da Silva, M. R. Meneghetti, J. M. Hickmann, *Appl. Phys. Lett.* **2008**, *92*, 201902.
[24] S. Köber, M. Salvador, K. Meerholz, *Adv. Mater.* **2011**, *23*, 4725.
[25] M. D. W. Grogan, S. C. Heck, K. M. Hood, S. A. Maier, T. A. Birks, *Opt. Lett.* **2011**, *36*, 358.
[26] D. D. Smith, L. Sibille, E. Ignont, R. J. Cronise, D. A. Noever, *J. Porous Mater.* **2000**, *7*, 499.
[27] G. Patermarakis, N. Nicolopoulos, *J. Catal.* **1999**, *187*, 311.
[28] I. A. Paun, V. Ion, A. Moldovan, M. Dinescu, *AIP Conf. Proc.* **2012**, *1464*, 547.